Testing and Status of the LSST Hexapods and Rotator

Ryan Sneed*[b], Douglas R Neill[a], Brendan Caldwell[b], Bryan Walter[b]
Harini Sundararaman[a], Mike Warner[a]
[a]Large Synoptic Survey Telescope, 950 N Cherry Ave., Tucson, AZ, USA 85719
[b]Moog CSA, 2581 Leghorn St., Mountain View, CA, USA 94043

ABSTRACT

The Large Synoptic Survey Telescope (LSST) is a large (8.4 meter) wide-field (3.5 degree) survey telescope, which will be located on the Cerro Pachón summit in Chile. Both the Secondary Mirror (M2) Cell Assembly and Camera utilize hexapods to facilitate optical positioning relative to the Primary/Tertiary (M1M3) Mirror. A rotator resides between the Camera and its hexapod to facilitate tracking. The hexapods and rotator have been designed, fabricated, assembled, and are currently being tested by Moog CSA. An update on these activities is provided along with a detailed discussion of the testing approach and results ranging from proof load and life testing to positioning performance. Particular emphasis is given to testing of the positioning accuracy, repeatability, and resolution of the hexapods and tracking accuracy and runout of the rotator. Verification of power off braking, heat dissipation, settling time, range of motion, and velocity requirements are also presented.

Keywords: LSST, hexapod, rotator, optical positioning

1. INTRODUCTION

This document presents an update on the status and a detailed discussion of the testing of the Secondary Mirror (M2) Cell Assembly hexapod and the Camera hexapod/rotator assembly of the Large Synoptic Survey Telescope (LSST). The document emphasizes the activities since the final design was completed[1]. The hexapods, hexapod actuators, and rotator designs are described in more detail in references 1 and 2.

The LSST[3, 4] is a large, ground-based telescope currently under construction that can survey the entire visible sky every three nights. This achievement is accomplished via a three-mirror telescope design consisting of an 8.4-meter Primary Mirror (M1), 3.4-meter Secondary Mirror (M2) and a 5.0-meter Tertiary Mirror (M3)[5] , Fig. 1. This system design accommodates a 3.5-degree field of view, feeding a large three-lens refractive Camera[6].

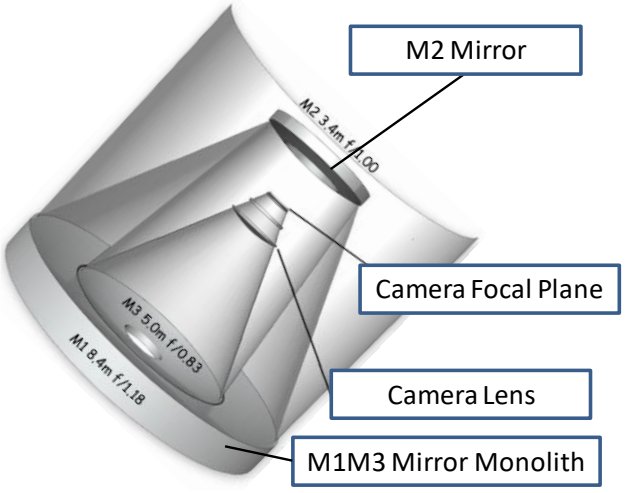

Figure 1: LSST Optical Configuration

Since the optical system, Fig. 1, does not include a fast steering mirror, the telescope has stringent vibration limitations during observation. This requires structurally efficient hexapods which produce high natural frequencies. The compact optical configuration also requires a compact camera hexapod/rotator design and limited hexapod motions.

*RSneed@moog.com; phone 1-303-216-9777 ext 219

Both the Secondary Mirror (M2) Cell Assembly[7] and Camera[6] utilize hexapods to facilitate optical positioning relative to the Primary/Tertiary (M1M3) Mirror[4], Fig. 2, which is required for active optics control[8, 9]. Geometric considerations preclude the use of a conventional hexapod arrangement for the M2 Hexapod. A rotator resides between the Camera and its hexapod to facilitate tracking. The requirements of the M2 Hexapod and Camera Hexapod are very similar; consequently to facilitate maintainability both hexapods utilize identical actuators.

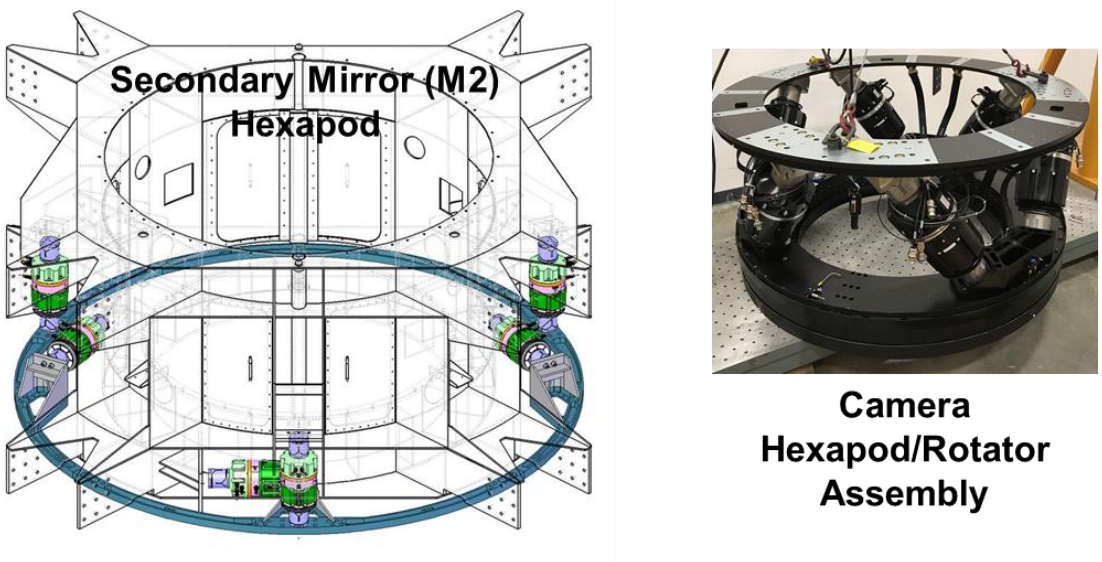

Figure 2: LSST M2 Hexapod (left) and Camera Hexapod/Rotator Assembly (right)

2. HEXAPODS AND ROTATOR STATUS

The final design review for the hexapods and rotator was successfully completed in October 2015. Following this milestone, procurement and fabrication of all components was begun in earnest for each of the subsystems. Critical components with long lead times were prioritized and these items included the roller screws and harmonic drives used in the hexapod actuators, the large machined interface plates/rings for both hexapods, and the ring and pinion gears and curved linear guide rails and carriages for the rotators. The hexapod actuator component procurement was completed first which allowed all 13 actuators (six for each hexapod and one spare) to be assembled in Moog's Mountain View, CA facilities by January 2017. Subsequently, all 13 actuators were tested individually as detailed below.

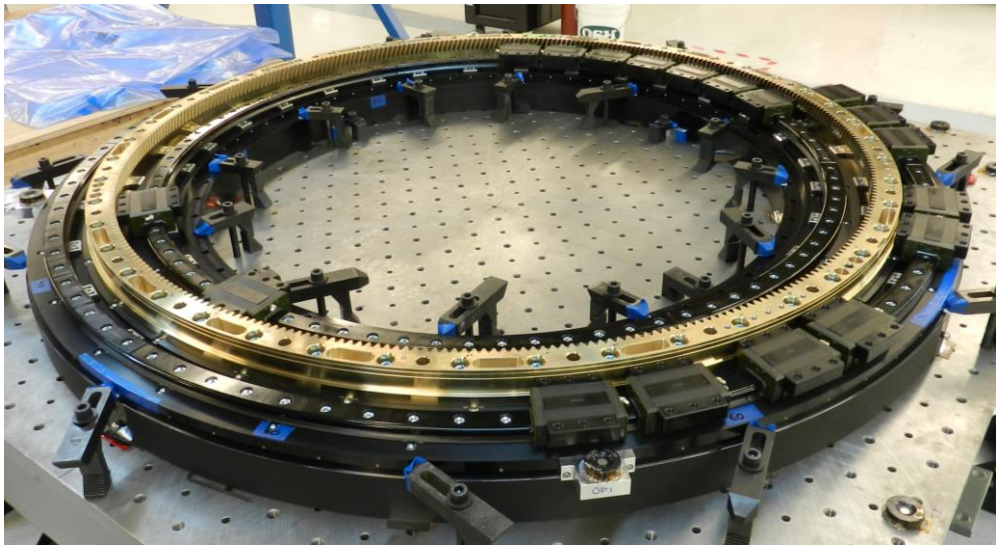

Figure 3: In-progress assembly of camera rotator

Rotator component procurement was completed in December 2016 to allow for the construction of two rotators with one serving as a spare. Assembly of the rotators was very challenging and required extensive laser tracker measurements and shimming to ensure the curved linear guide segments were assembled to the necessary flatness, parallelism, circularity, and concentricity to avoid binding and allow for low friction motion. Assembly was also performed at 61 deg F to minimize thermal-induced stresses across the expected temperature range. Assembly of the two rotators was completed in April 2017 and September 2017, respectively. Following preliminary motion control software integration and checkouts, the first rotator was integrated with six camera hexapod actuators and the associated structural components to form the complete camera hexapod/rotator assembly in June 2017. The camera hexapod/rotator assembly was mounted to a large test frame in Moog's facilities in Golden, CO to allow for testing at elevation angles ranging from 0 to 90 degrees. Following control system tuning of both the hexapod and rotator, acceptance testing was completed from October 2017 to February 2018 culminating with a successful acceptance review. The first rotator was then de-integrated from the camera hexapod and replaced with the second rotator. Full acceptance testing was then repeated on the second rotator with completion in March 2018.

Fabrication of the main M2 hexapod structural components was completed in October 2017 although they have been stored at the fabricator's facility until assembly of the M2 hexapod begins in April 2018. Acceptance testing of the M2 hexapod is expected to be completed in May 2018. Final software testing verifying interfaces with the Telescope Control System is scheduled for June 2018 with delivery to the telescope site the following month.

3. HEXAPOD AND ROTATOR TESTING

To reduce risk and identify any manufacturing or assembly errors, all hexapod actuators were tested individually prior to being assembled into either hexapod. Similar component-level testing was not practical for the rotator aside from stiffness and friction testing of the bearing elements. The camera hexapod and rotator share structural components, and consequently, they were tested together as a complete assembly.

3.1 Hexapod Actuator Testing

The hexapod actuators were tested to ensure their individual performance would be sufficient to meet the system-level requirements of both the camera hexapod and M2 hexapod. The test setup consisted of a pneumatic cylinder and precision air regulator to provide loading forces which were measured with a 50,000 lb load cell. Two high resolution encoders provided absolute position measurements from one end of the actuator to the other and their readings were averaged. A linear guide was attached to the moving end of the hexapod actuator to maintain alignment with the pneumatic cylinder. Tests were performed on each actuator to ensure compliance with the following requirements: backdriving, stiffness, resolution, repeatability, and accuracy. The spare actuator was subjected to more extensive testing along with an

accelerated life test. Performance tests were repeated on the spare actuator after the life test to confirm that there were no significant deviations in behavior.

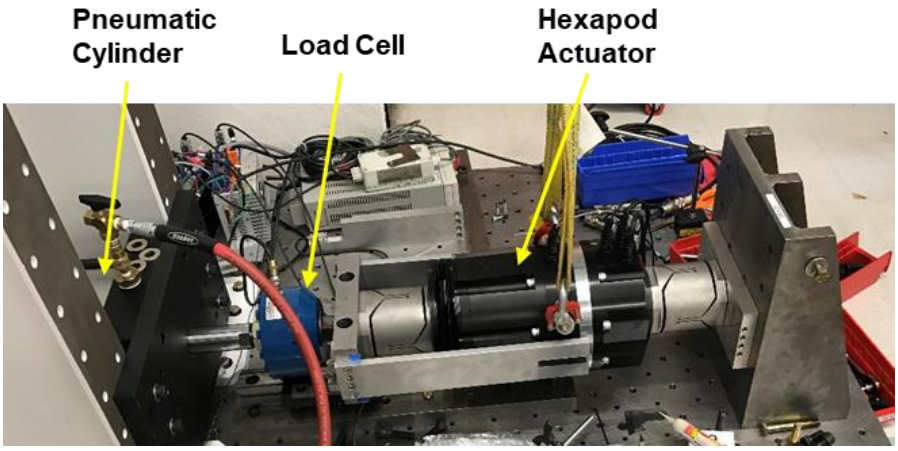

Figure 4: Hexapod actuator test set-up

3.1.1 Backdriving

The hexapods are not allowed to backdrive. To minimize heat dissipation which could impact the telescope's image quality, the hexapod actuators do not use brakes. However, the fine pitch of the roller screw decreases its efficiency to the extent that they are self-locking[1]. The harmonic drive gear reducer in the actuators provides additional resistance to backdriving. To confirm that backdriving would not occur, a 60 kN load was applied to the actuators in both tension and compression. This represented 2X the maximum expected loading during operation to ensure backdriving would not occur when subjected to potentially higher loads during maintenance operations or during proof load testing described below.

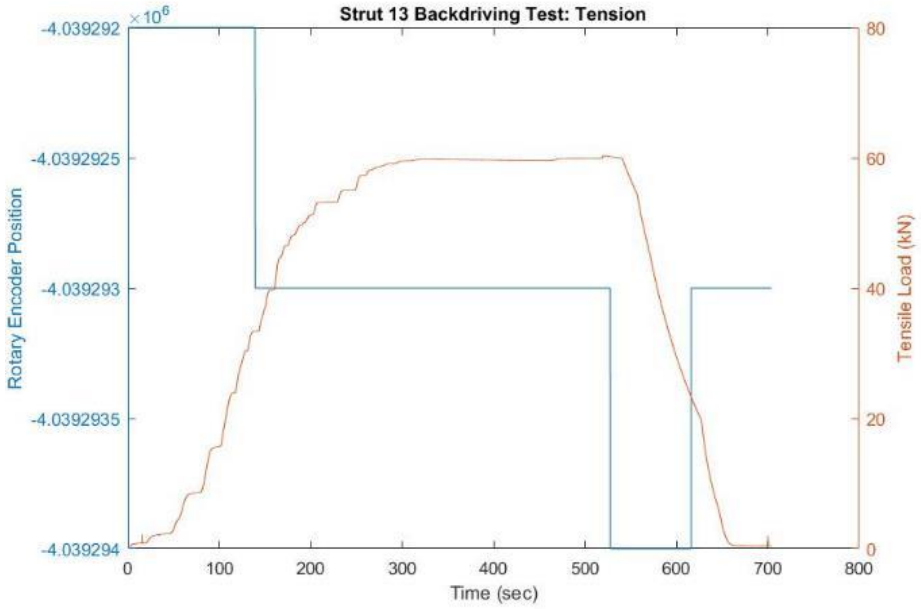

Figure 5: Hexapod actuator backdriving test results showing no significant change in motor encoder position (in counts)

The motor encoders were monitored during the test to ensure the screw was not turning. The largest motion observed was two encoder counts which corresponds to 4nm of linear motion. This motion is negligible and not representative of backdriving.

3.1.2 Stiffness

Actuator axial stiffness was a major factor in maintaining all natural frequencies of the camera hexapod/rotator assembly above the 16 Hz requirement. The stiffness was tested by measuring the deflection of the actuator as loads were applied up to 30 kN in tension and 30 kN in compression which corresponds to the maximum loading range during operation. The compliance introduced by test rig itself was assessed by measuring an aluminum cylinder with a known stiffness in the same manner. The series stiffness contributed by the test rig could then be determined and factored out of the actuator stiffness results. The effective test rig stiffness was over 100X greater than the actuator stiffness being measured, so it contributed only a 1% reduction in the measured stiffness.

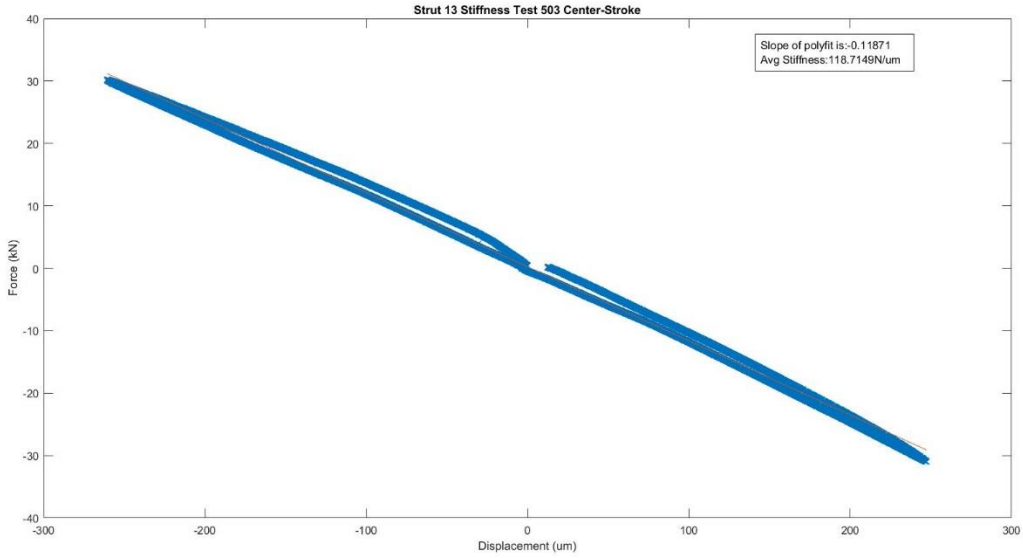

Figure 6: Hexapod actuator stiffness test results showing stiffness of 119 N/µm

The actuator axial stiffness was predicted to be 134 N/µm based on a combination of finite element analysis and component-level stiffness measurements. The average measured stiffness of the actuators was 118.9 N/µm at the center of stroke position after factoring out the compliance from the test fixtures. This was 11.3% lower than predicted, but was determined to be adequate for meeting the natural frequency performance. The stiffness of all 13 actuators measured within 4% of this average value which added confidence that there were no manufacturing or assembly errors. The deviation between the measured stiffness at the center stroke, fully extended, and fully retracted actuator positions was also within 1.5% as expected. The linearity of the measurements was good over the entire load range although there is small, but observable hysteresis. The hysteresis likely originated from the cross roller bearing used in the actuator.

3.1.3 Resolution

Kinematic analysis of the camera hexapod and M2 hexapod determined that if the hexapod actuators were capable of 100 nm resolution, all six of the hexapod-level resolution requirements for both systems could comfortably be met. Resolution was tested by taking several 100 nm steps in both the extending and retracting directions and comparing the test encoder readings to the readings from the actuator's internal encoder. Tests were performed at representative loads of 15 kN in both tension and compression. In all cases the actuator's encoder shows motion in the commanded direction and an appropriate step size close to 100 nm. The test encoders contain significant noise due to their mounting configuration, but also show motion in the appropriate direction with reasonable step sizes.

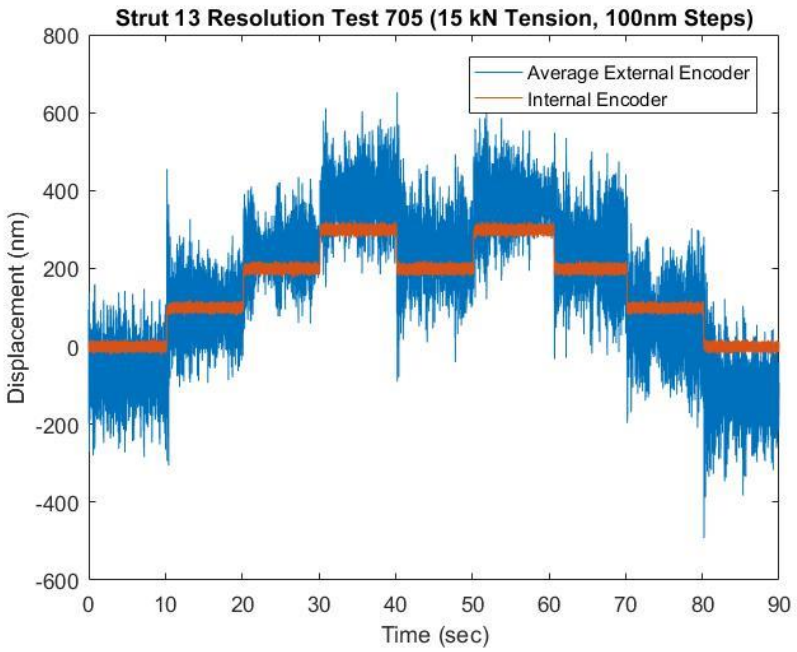

Figure 7: Hexapod actuator resolution test results for 100 nm steps

3.1.4 Repeatability

Repeatability testing was performed by moving from the zero position to a positive position, back to zero, to a negative position, back to zero, and repeating the sequence several times. The step size for these moves was chosen to be 0.5 mm since that represented a large displacement compared to typical moves sizes during actual telescope operation. The repeatability is the deviation in position between all of the steps to the same positions. The unidirectional repeatability (always moving from the same direction) was within 1 µm and the bi-directional repeatability (moving from either direction) was within 3 µm. These results were considered excellent performance and were sufficient for meeting the hexapod-level repeatability requirements in all axes based on kinematic analysis of both hexapods.

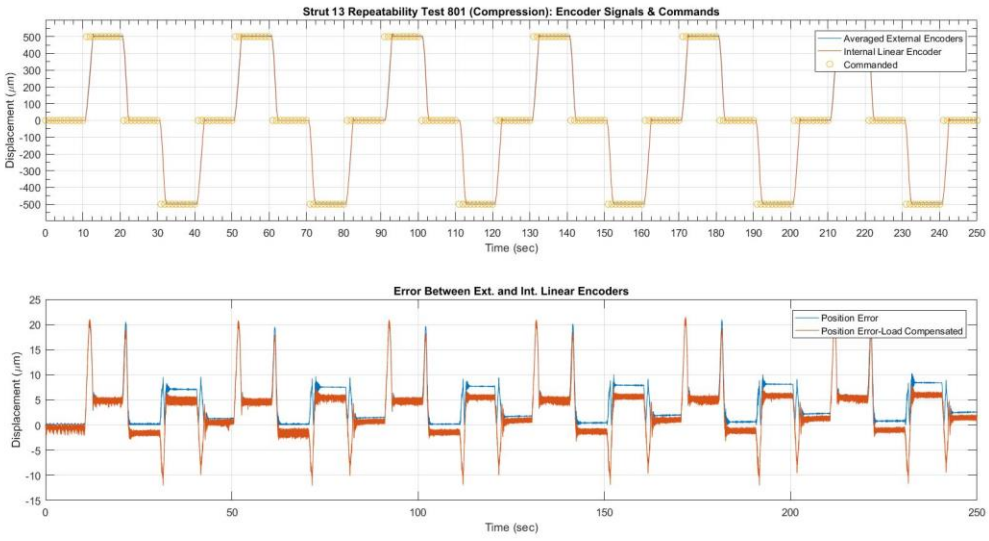

Figure 8: Hexapod actuator repeatability for 0.5 mm steps was within 3 µm for bi-directional steps and within 1 µm for uni-directional steps

3.1.5 Accuracy

Actuator accuracy was tested by making several position commands across the entire range of motion and calculating the difference between the actuator's encoder measurements and the test encoder measurements. The tests were performed with representative 15 kN loads in both tension and compression. However, the pneumatic cylinder did not maintain a perfectly consistent load as the actuator changed position, so load compensation was performed to remove compliance-related position changes that would be measured by the test encoders, but not the actuator's encoder.

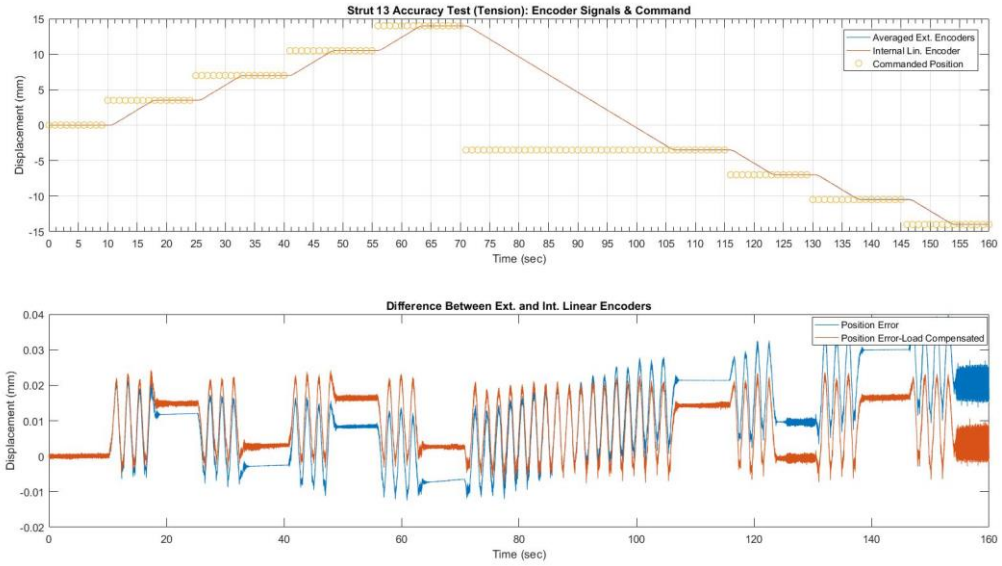

Figure 9: Hexapod actuator accuracy results showed errors less than 20 µm across entire range of motion

The positioning accuracy errors of the actuator were within 20 µm across the entire range of motion and kinematic analysis showed that these error level would be sufficient to meet the hexapod-level accuracy requirements in all six axis for both hexapods. The actuators were expected to have this excellent level of positioning accuracy because they have a high accuracy linear encoder on the screw rather than relying on motor encoder measurements[1].

3.2 Camera Hexapod Testing

Acceptance testing of the camera hexapod began with proof load testing followed by an accelerated 1 year life test before beginning the primary performance testing. Proof load testing was performed first so that any damage that was not otherwise obvious would be identified in subsequent performance testing. The life test was also performed prior to performance testing to identify any infant mortality failures, but also so the actuators were appropriately worn in when tested. The performance testing was executed with a 1.25X payload mass to ensure adequate performance with the coolant, power, and communication cables of the camera contributing additional and difficult to predict loads on the hexapod.

3.2.1 Proof Testing

Proof testing was performed with a payload mass 2X larger than the actual camera mass of 3060 kg. Additional weights were added to a surrogate payload structure in an arrangement that did not significantly shift the center of mass of the payload. The load was applied for 10 minutes at 0 deg elevation angle (worst case actuator loading) and slowly rotated to 90 deg elevation angle where it was maintain for another 10 minutes. The test was considered successful due to the lack of unexpected movement or sounds that would indicate a catastrophic failure.

Figure 10: Proof load testing of the camera hexapod and rotator with a 2X payload mass at a 90 deg elevation angle

3.2.2 Life Testing

Life testing of the hexapod consisted of executing position commands produced by telescope simulations that were consistent with expected movements during 10 typical nights of telescope observations. The commands were repeated 36.5 cycles to represent an entire year of motion. The dwell time between moves was reduced from 30 seconds to 1 second to allow the test to be completed in approximately 2 weeks. The test was executed with the nominal 1X payload mass and was successfully completed without unexpected stoppages or obvious signs of wear or damage.

3.2.3 Power Off Braking/Backdriving

To confirm that the hexapod had power off braking capability and would not backdrive, the motor power cables were disconnected from all six actuators to ensure no power was being applied to the motors. Under worst case loading at 0 deg elevation angle, the actuator encoder positions were recorded before and after being left unpowered overnight. The maximum deviation in actuator position was less than 0.3 µm. This very small deviation was expected due to thermal shifts and demonstrated that backdriving had not occurred. This result was expected based on individual actuator testing, but needed to be confirmed for the fully assembled hexapod.

3.2.4 Range of Motion

With the center of rotation set 2.7584 meters away from the hexapod origin in the z-direction (corresponding to the camera L1 vertex), it was demonstrated that the range of motion requirements shown in Table 1 could be achieved simultaneously by moving to 32 different combinations of this maximum range. This was done without activating any actuator limit switches or software range limits. Since RZ-axis motion is only used for diagnostic testing, it was not included in the simultaneous range requirements.

Table 1: Camera hexapod simultaneous range of motion

	XY-Axes	Z-Axis	RXRY-Axes	RZ-Axis
Simultaneous Range	±5.66mm	±7.73mm	±0.17deg	±0deg

With all off-axis displacements and rotations at zero, it was demonstrated that the ranges of motion shown in Table 2 could be achieved independently. A laser tracker was used to confirm that these displacements and rotations were achieved within the accuracy requirements of the particular axis of motion. Although the hexapod has additional range capacity beyond these values, extended displacements and rotations were not expected to be useful for the telescope's operation, so consequently, the control software limits displacements and rotations to these values.

Table 2: Camera hexapod independent range of motion

	XY-Axes	Z-Axis	RXRY-Axes	RZ-Axis
Independent Range	±11.4mm	±13.1mm	±0.36deg	±0.1deg

3.2.5 Slewing and Settling Time

The hexapod is required to execute small hexapod motions (less than 150 µm axial motion, 200 µm radial motion and 0.004 deg tilts in any combination) within 2 seconds and then settle within its positioning requirements within another 2 seconds. This was confirmed by commanding several representative combined moves of the maximum sizes and verifying that both the slewing time and settling time were always within 1.82 sec and 1.19 sec, respectively. It was also confirmed that large slews settle within a similar time duration.

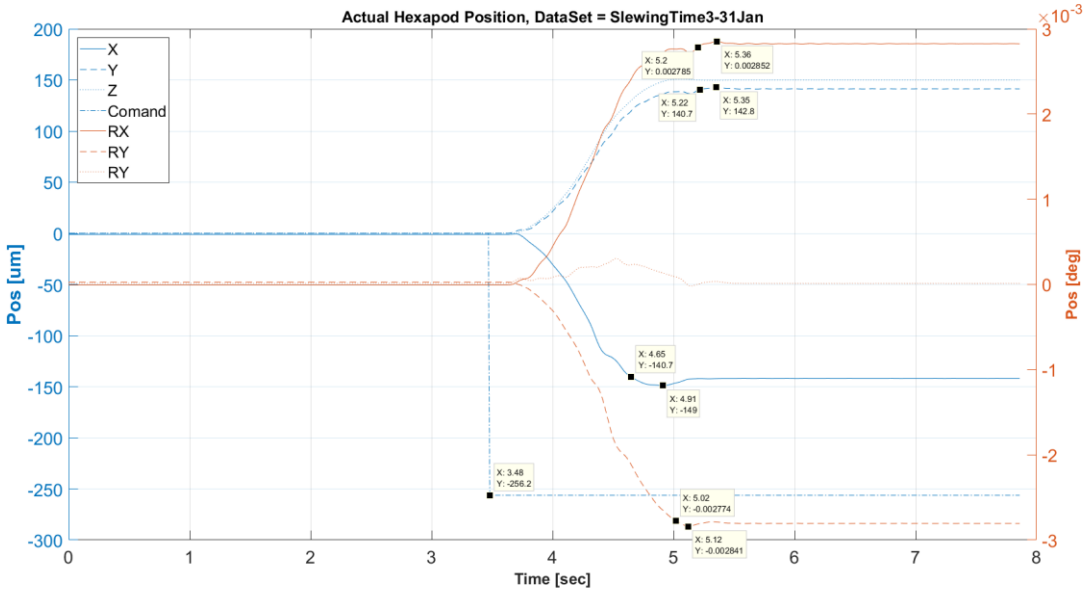

Figure 11: Camera hexapod slewing and settling time test results show slewing and settling each within 2 seconds

3.2.6 Resolution

Camera hexapod resolution was tested by commanding two consecutive moves of the desired resolution step size in the positive direction, followed by a move in the negative direction, followed by a move in the positive direction, followed by a move in the negative direction. This ensured that the system can provide the necessary resolution when changing direction which is generally more difficult for positioning systems. The actual motion was measured with two high resolution length gauges. A move was considered successful if it moved in the commanded direction and the magnitude of the move was within 50% of the commanded value.

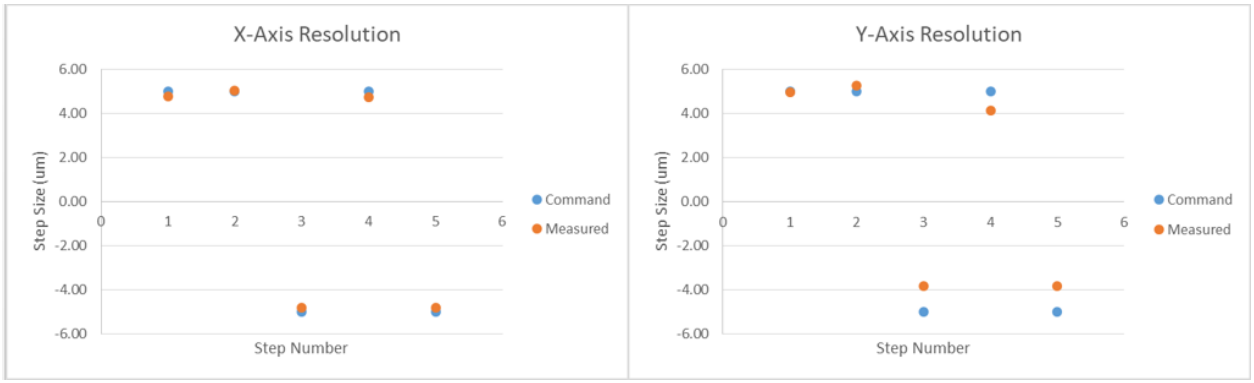

Figure 12: Resolution test results for X and Y-axes of camera hexapod

Table 3: Confirmed camera hexapod resolution in all axes

	XY-Axes	Z-Axis	RXRY-Axes	RZ-Axis
Resolution	5 µm	1 µm	1.4 µrad	10 µrad

The camera hexapod was shown to have the required resolution shown in Table 3. Testing was performed with the camera hexapod oriented at a variety of elevation angles to ensure the resolution performance was achievable under conditions similar to on-telescope operation.

3.2.7 Repeatability

Camera hexapod repeatability was tested by commanding a representative step size move in one direction, then back to the starting position, the same step size move in the opposite direction, then back to the starting position, and repeating the process three times. The actual positions were measured with length gauges and the repeatability was the maximum deviation between the measurements at each of the same commanded positions.

Table 4: Camera hexapod repeatability requirements and measurement performance in all axes

Axis	Step Size	Required Repeatability (um, deg)	Measured Repeatability at El Angle #1 (um, deg)	Measured Repeatability at El Angle #2 (um, deg)
X	100 um	20	5.55	2.7
Y	100 um	20	7.46	3.13
Z	50/100um	5	1.29	3.61
RX	0.0015	0.0003276	0.000286	0.000232
RY	0.0015	0.0003276	0.000215	0.000163
RZ	0.015	0.0024	0.00064	0.00037

A summary table of the repeatability test results is provided in Table 4. Testing was performed with the camera hexapod oriented at a variety of elevation angles to ensure the repeatability performance was achievable under conditions similar to on-telescope operation.

3.2.8 Accuracy

Camera hexapod accuracy was tested by commanding moves to 25%, 50%, 75%, and 100% of the full scale range in the positive direction and then 25%, 50%, 75%, and 100% in the negative direction for each axis. The actual positions were measured with a combination of a laser tracker and length gauges and the accuracy was computed as the largest deviation from the command. A summary table of the accuracy test results is provided in Table 5.

Table 5: Camera hexapod accuracy requirements and measured performance in all axes

Axis	Required Accuracy (um, deg)	Measured Accuracy El Angle #1 (um, deg)	Measured Accuracy El Angle #2 (um, deg)
X	125	124.06	55
Y	125	124.98	42
Z	25	20	15
RX	0.0020475	0.002	0.002
RY	0.0020475	0.002	0.002
RZ	0.015	0.0027	0.002

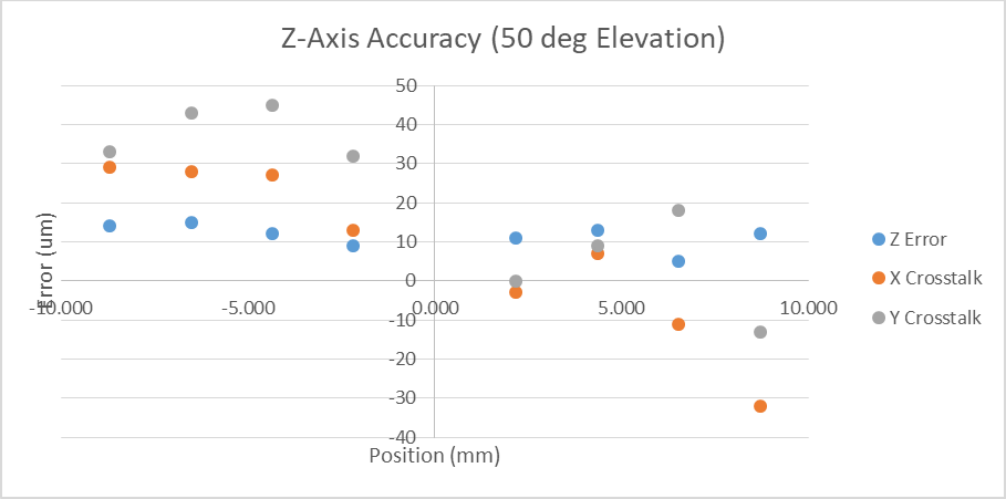

Figure 13: Camera hexapod z-axis accuracy measurements including x and y-axes crosstalk measurements

In addition to measuring accuracy of motion in the commanded axis, crosstalk or motion in the non-commanded axes was also measured where practical. The Z-axis accuracy test results, shown in Figure 13, include crosstalk measurements in X and Y. The crosstalk errors must also be within the accuracy requirement of each axis and this was demonstrated during testing. Testing was again performed with the camera hexapod oriented at a variety of elevation angles to ensure the accuracy performance was achievable under conditions similar to on-telescope operation.

3.2.9 Velocity

While the camera hexapod is used for static positioning and is relatively slow moving by design, the system needs to be able reposition the camera quickly enough to avoid interfering with the telescope's required operation rate. The camera hexapod comfortably exceeded the simultaneous velocity requirements shown in Table 6 for a variety of multi-axis commands.

Table 6: Camera hexapod simultaneous velocity required in all axes

	XY-Axes	Z-Axis	RXRY-Axes	RZ-Axis
Velocity	152 µm/s	152 µm/s	0.0039 deg/s	0.0039 deg/s

3.2.10 Heat Dissipation

Camera hexapod actuator heat dissipation was measured by placing inductive current probes on each of the three motor phase lead wires to measure the three phase currents. The phase currents were used to generate time histories of the motor heat loss and mechanical power, and the combined results were averaged and multiplied by the expected duty cycle of 6.25%. Under the worst-case expected loading and travelling at the maximum speed, the average motor power dissipated was 1.66 Watts. This value was added to the small amount of heat dissipated by the actuator's encoders to determine the maximum actuator heat dissipation was 3.0 Watts. This value was well inside the required heat dissipation limit of 10 Watts per actuator.

3.3 Rotator Testing

Similar to the camera hexapod, acceptance testing of the rotator began with proof load testing followed by an accelerated 1 year life test before beginning the primary performance testing. Since the camera hexapod and rotator form a single assembly, the proof load and life testing of the rotator was performed simultaneously with the camera hexapod as described above. The performance testing was also executed with a 1.25X payload mass to ensure adequate performance with the coolant, power, and communication cables of the camera contributing additional and difficult to predict loads on the rotator. After completion of acceptance testing on the first rotator, it was removed from the camera hexapod and replaced with the second rotator. Both rotators were subjected to identical testing. Results shown below were for the first rotator, but the performance of the second rotator was comparable.

3.3.1 Absolute Accuracy and Range

Rotator absolute accuracy was measured with a laser tracker by measuring the position of a target located near the outer diameter of the rotator every 30 deg across the entire ±90 deg range of motion. The data was fitted to a best fit circle which was used to determine the angular rotations. Four reference targets were used on the non-moving side of the rotator to compensate for movement of the test structure at each location.

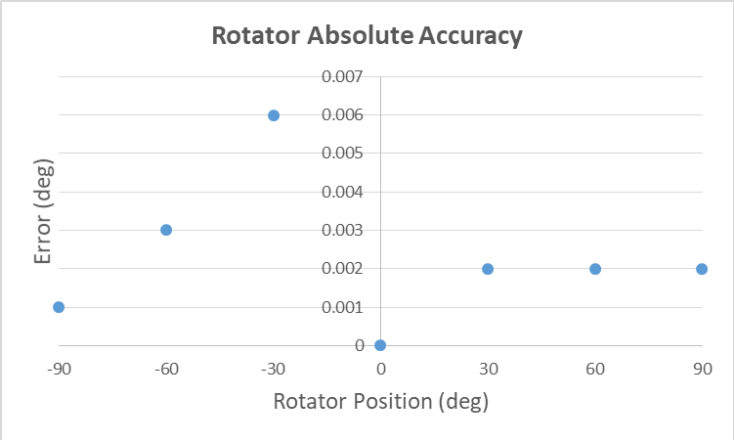

Figure 14: Rotator absolute accuracy measurements over entire ±90 deg range of motion

The maximum angle error was 0.006 deg which was within the required value of 0.009 deg.

3.3.2 Velocity and Acceleration

A large rotator motion of 30 deg was commanded in each direction that would allow the rotator to reach its maximum velocity. The velocity was measured by differentiating the rotator load encoder signal and looking at the maximum velocity achieved after the acceleration period was complete. The rotator maintained a constant 3.5 deg/s in both directions which was the required level and also corresponded to the velocity limit enforced by the control software.

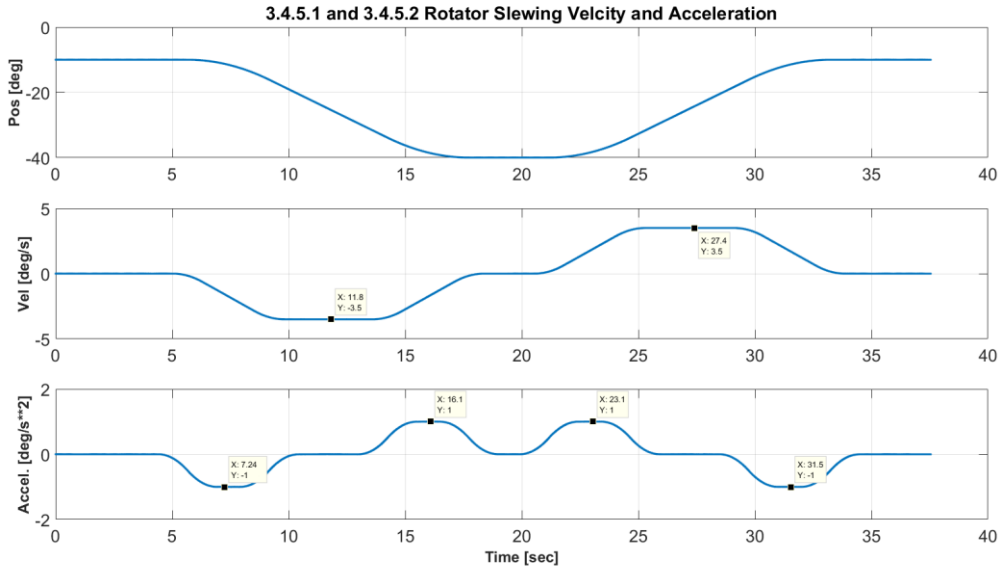

Figure 15: Rotator maximum velocity and acceleration measurements during a large rotation

The acceleration was measured during the same rotator motion by twice differentiating the rotator load encoder signal and determining the maximum acceleration level achieved after the ramp up (ie, jerk) period was complete. The rotator achieved a 1.0 deg/s^2 level during all acceleration and deceleration periods which was the required level and also corresponded to the acceleration/deceleration limit enforced by the control software.

3.3.3 Run-out

The rotator run-out was measured across the entire range of motion using a laser tracker to measure the position of a target on the moving side of the rotator at every 10 degree increment except where line-of-sight was blocked by the payload. The radial run-out was the deviation from a best fit cylinder formed from all of the data points. The maximum radial run-out was 49 µm which was within the 50 µm requirement. The axial run-out was the deviation from a best fit plane formed from all of the data points. The maximum axial run-out of 87 µm was also within the required limit of 100 µm.

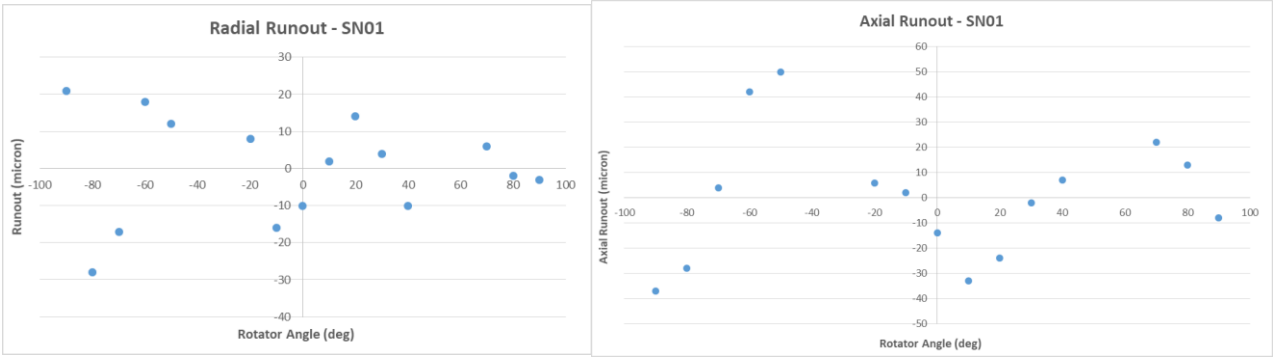

Figure 16: Rotator radial (left) and axial (right) run-out

Non-repeatable axial run-out is problematic because it creates focus errors that cannot be removed with a look-up table. Non-repeatable axial run-out was measured with eddy current probes mounted from the fixed side of the rotator and sensing on the face of the moving side. The sensors measure not only axial run-out but also surface finish and surface flatness variations of the sensed plate. Fortunately, the last two contributions are repeatable. The test was executed seven times moving the rotator through the entire 180 deg range. The first six data sets were averaged together to create a mean displacement profile. The seventh data set was differenced with the mean displacement profile to leave the non-

repeatable run-out. The root mean squared (RMS) of the non-repeatable axial run-out from each eddy current probe was less than 1 µm over the total range compared to the allowable value of 2 µm.

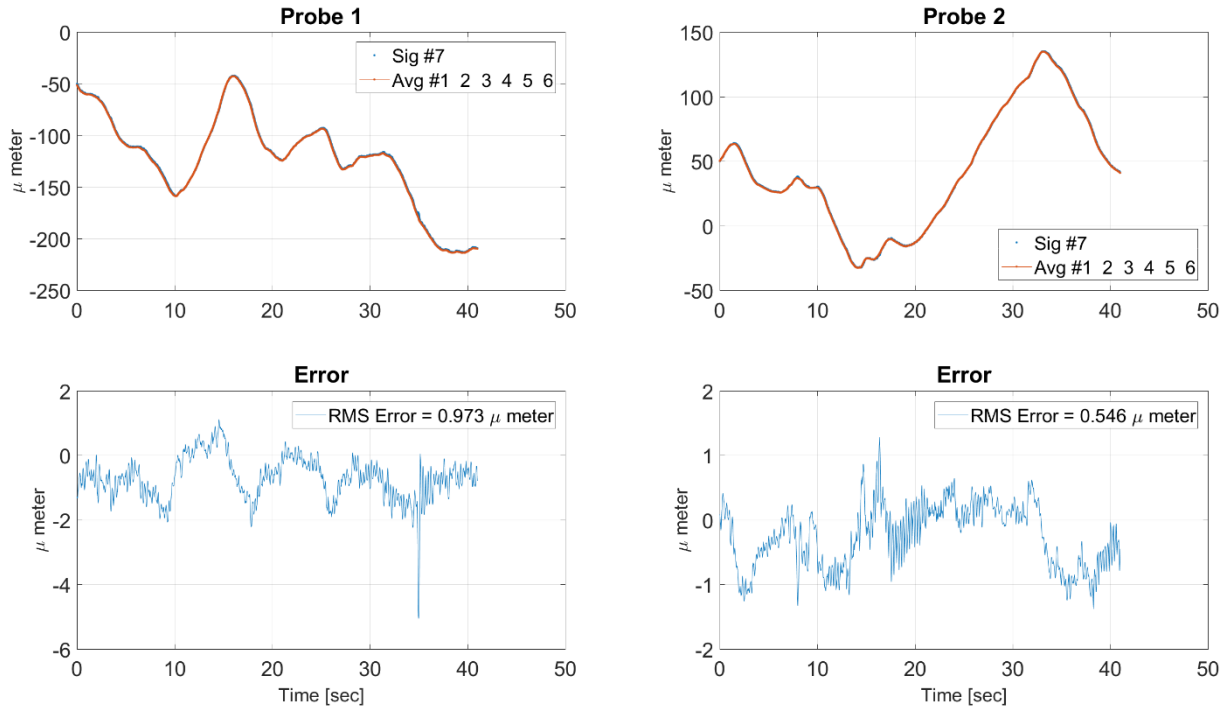

Figure 17: Total measured axial displacements (top) and non-repeatable axial runout (bottom) measured from two separate sensors over the entire rotator range of motion

Run-out is especially important over rotator ranges of 1 deg or less which correspond to the rotator motion during the 15 second baseline exposure of the LSST camera. Non-repeatable radial run-out is problematic because it creates motion of the image on the 10 µm pixels of the LSST camera detector. To measure radial run-out over these small intervals, two eddy current probes located 180 deg apart were mounted from the fixed side of the rotator and sensed on the outer diameter of the moving side. Unfortunately, the eddy current probes measure not only the radial runout, but also the surface finish and out-of-round of the plate. A practical means for extracting these factors from the radial runout could not be found, but run-out was indicated by the measurements from the two probes moving in opposite directions (rotating plate moves towards one sensor and away from the other sensor). Data was taken over the entire 180 deg range and a representative 1 deg slice is shown in Figure 18.

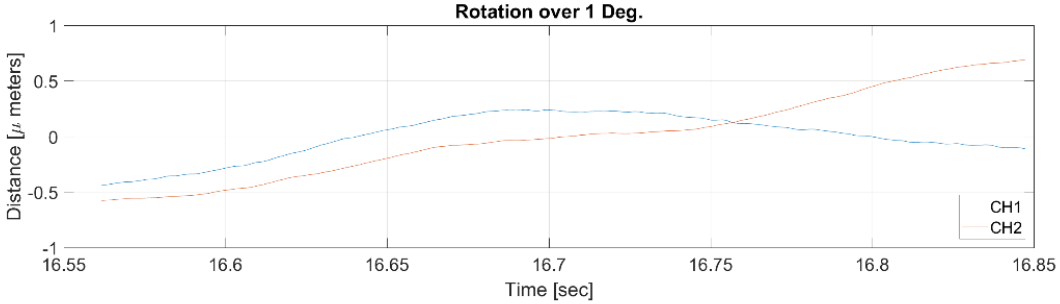

Figure 18: Rotator radial run-out over a 1 deg range

Measured displacement over the 1 deg range was ~1 µm peak-to-peak or ~0.5 µm RMS. While it was not possible to precisely quantify the radial run-out from these measurements, most of the motion was in the same direction on both opposing sensors indicating that the radial run-out was below the requirement of 0.5 µm RMS.

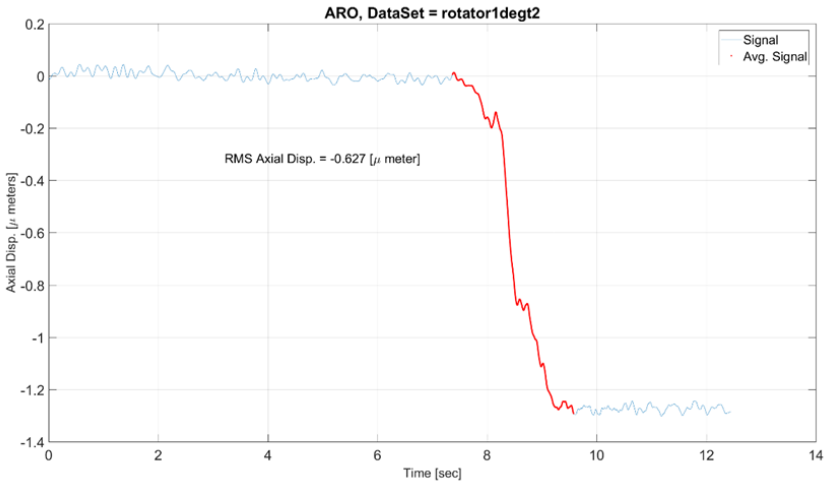

Figure 19: Rotator axial run-out over a 1 deg range

Axial run-out over a 1 deg interval was measured with a laser interferometer. The measurement optic was placed close to the rotation axis to avoid including tilt axis errors in the measurements. The measurements included any motion of the test frame which added error to the results, but the axial run-out was less than the 1 µm RMS limit for the several intervals which were measured.

3.3.4 Tracking Accuracy

Rotator tracking accuracy was measured for constant velocity commands ranging from 0.005 deg/s to 0.068 deg/s in both directions. The rotator's internal encoder measurements were recorded over the 15 second baseline (ignoring start-up transients) and the RMS position error jitter was computed relative to the command. The test was performed at three different velocities at each of five different elevation angles for a representative sample. As shown in Table 7, the tracking errors were generally higher at higher velocities, but all values were within the requirement of 0.481 µrad RMS

Table 7: Summary of rotator tracking errors

	Rotator Tracking Accuracy (urad RMS)				
Tracking Velocity (deg/s)	20 Deg El	35 Deg El	50 Deg El	65 Deg El	80 Deg El
-0.068		0.444			
-0.05				0.358	
-0.04			0.29		
-0.03	0.267				
-0.02					0.177
-0.01		0.107			
-0.005				0.074	
0.005	0.067				
0.01					0.108
0.02				0.169	
0.03			0.248		
0.04		0.317			
0.05	0.347				0.280
0.068			0.423		

While the rotator's internal encoder measurements were expected to be very high fidelity, verification from external metrology was needed to confirm these measurements. A laser interferometer was used at 0 deg elevation angle (the laser head can only be aligned at 0 and 90 deg elevation angles) for external confirmation, but since the laser interferometer head was supported on a tripod resting on the lab floor, any movement of the test frame would be included in the measurements along with any ambient noise from the laser interferometer. The tracking accuracy requirements apply only to the rotator itself since motion of the telescope structure was accounted for elsewhere. To be able to remove all other error sources from the measurements, an additional set of laser interferometer measurements was taken from the fixed side of the rotator, and the RMS error was removed from the measurements on the moving side

of the rotator by root sum squared method. Using this approach the laser interferometer tracking accuracy measurements matched the rotator's internal encoder measurements within 20-30%.

3.3.5 Heat Dissipation

Rotator heat dissipation was measured by placing inductive current probes on each of the three motor phase lead wires to measure the three phase currents. The phase currents were used to generate time histories of the motor heat loss and mechanical power, and the combined results were averaged. The tests were performed at three different representative combinations of elevation angle and tracking velocities to replicate average usage conditions although the heat dissipation was similar in all three cases. The average motor power dissipated for the drive motor and bias motor were 8.6 W and 0.3 W, respectively. This was added to the measured motor brake power consumption of 9.38W per motor and the small amount of power consumed by the motor encoders and load encoders. The total rotator heat dissipation was 30.35 W which was within the allowable value of 40 W.

3.4 M2 Hexapod Testing

M2 hexapod testing has not yet begun at time of writing. Since the M2 hexapod is a stand-alone assembly, it will be tested independently from the camera hexapod and rotators. The M2 hexapod testing will follow a very similar pattern to that of the camera hexapod. It will begin with proof load testing with a 2X payload mass followed by life testing with a 1X payload mass before moving into the bulk of the positioning performance testing with a 1.25X payload mass. There is very high confidence that the M2 hexapod will pass all of its performance tests based on the successful testing of the camera hexapod which uses identical actuators and has comparable positioning requirements. Although the M2 hexapod has a larger nominal payload mass of 5071 kg compared to the camera hexapod payload mass of 3060 kg, the actuators experience similar loading due to the significantly different geometry of the hexapods. This adds to the confidence that the M2 hexapod will achieve the required performance.

4. CONCLUSION

Procurement and fabrication of the camera hexapod, rotators, and all M2 hexapod components has been completed. Risk reduction testing of all hexapod actuators was completed and the results provided confidence that all camera hexapod and M2 hexapod requirements could be achieved. Acceptance testing of the camera hexapod and rotators has been completed with both systems meeting all major performance requirements. Assembly and acceptance testing of the M2 hexapod is expected to be completed by the end of May 2018 followed by delivery of all systems in July 2018.

5. ACKNOWLEDGMENT

This material is based upon work supported in part by the National Science Foundation through Cooperative Support Agreement (CSA) Award No. AST-1227061 under Governing Cooperative Agreement 1258333 managed by the Association of Universities for Research in Astronomy (AURA), and the Department of Energy under Contract No. DEAC02-76SF00515 with the SLAC National Accelerator Laboratory. Additional LSST funding comes from private donations, grants to universities, and in-kind support from LSSTC Institutional Members.

6. REFERENCES

[1] Sneed, R., Neill, D., Kidney, S., Araujo, C., Gressler, W., Lotz, P., Mills, D., Sebag, J., Sebring, T., Warner, M., Wiecha, O., "Final design of the LSST hexapods and rotator," Proc. SPIE 9906-18, (2016)
[2] Neill, D., Sneed, R., Dawson, J., Sebag, J., Gressler, W., "Baseline design of the LSST hexapods and rotator," Proc. SPIE 9150, (2014)
[3] Ivezic, Z. et al., "LSST: from Science Drivers to Reference Design and Anticipated Data Products," ArXiv e-prints arXiv:0805.2366 (2008).
[4] Gressler, W., "LSST telescope and site status," Proc. SPIE 9906-19, (2016)
[5] Araujo, C., Thomas, S. "Overview of the LSST Mirror System," Proc. SPIE 9906-20, (2016)
[6] Kurita, N., "Large Synoptic Survey Telescope Camera Design and Construction," Proc. SPIE 9912-27, (2016)
[7] Neill, D., Bogan, G. et al, "Final design of the LSST secondary mirror assembly," Proc. SPIE 9906-18, (2016)
[8] Neill, D., Angeli, G., Claver, C., Hileman, E., DeVries, J., Sebag, S., Xin, B., "Overview of the LSST active optics system," Proc. SPIE 9150, (2014)
[9] Thomas, S., "LSST AOS software architecture," Proc. SPIE 9906-18, (2016)